Distortion Analysis of Ultra-Wideband OFDM Receiver Front-Ends

Mahim Ranjan, *Member, IEEE*, and Lawrence E. Larson, *Fellow, IEEE*

***Abstract*—This paper presents a comprehensive analysis of the effect of nonlinearities in ultra-wideband orthogonal frequency-division multiplexing receivers. The statistical properties of a quadrature phase-shift keying baseband signal are utilized to derive closed-form expressions for the power spectral density of cross-modulation, intermodulation, and harmonic distortion products of modulated signals, arising from second- and third-order nonlinearities in the receiver. Both narrowband and wideband jammers are considered. The derived expressions are then used to predict the effect of these nonidealites on the link budget of the system.**

***Index Terms*—Cross-modulation, distortion, nonlinear circuit, orthogonal frequency-division multiplexing (OFDM), spectral analysis, statistics, ultra-wideband (UWB).**

I. Introduction

ULTRA-WIDEBAND (UWB) orthogonal frequency-division multiplexing (OFDM) systems have been proposed as an emerging solution to wireless communication applications requiring high data rates (up to 400 Mb/s) over short distances. In one proposed version [1], the carrier with a bandwidth of 528 MHz can hop to one of 14 channels ($2904 + 528n$ MHz, $n = 1, 2, \ldots, 14$), divided into four groups of three channels and one group of two channels. This representative time-frequency interleaving for a Group 1 only system is depicted in Fig. 1.

Since the front-end possesses a wide bandwidth, it is open to reception of undesired narrowband signals such as 802.11 a/b/g and the recently proposed WiMax [2] systems, as shown in Fig. 2. Although OFDM systems are less susceptible to relatively narrowband jammers, nonlinearities in the receiver can result in these narrowband jammers cross-modulating with wideband signals present at the input, resulting in reduced signal-to-noise ratio (SNR) and, ultimately, a degradation in system performance [3]. In addition, wideband signals (from other UWB transmitters) can intermodulate and the resulting products can land in a desired channel. Since the system is inherently wideband, harmonic distortion of a single unwanted UWB transmitter can also produce in-band distortion products

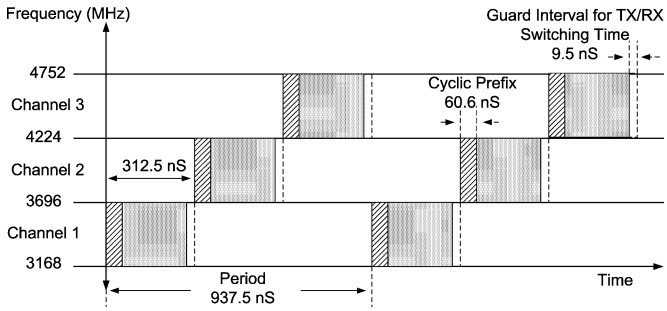

Fig. 1. Time-frequency interleaving of a Group 1 MB-OFDM signal [1].

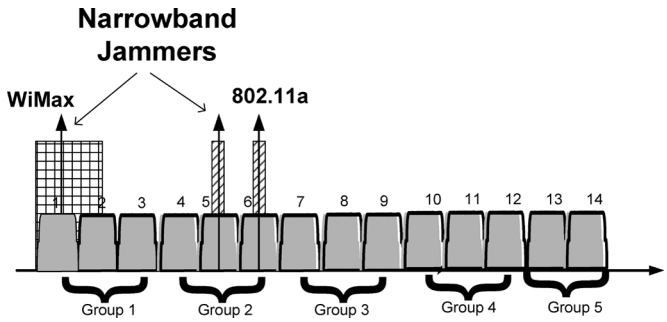

Fig. 2. Representative spectrum at MB-OFDM receiver input.

and reduce SNR. While cross-modulation in code-division multiple-access (CDMA) and wideband code-division multiple-access (W-CDMA) receivers has been extensively studied [6], [7], cross-modulation distortion of a narrowband jammer and a UWB interferer at the receiver input due to third-order nonlinearity was presented in [3]. This paper extends our study in [3] to analyze the effects of multiple UWB jammers at the receiver input due to both second- and third-order nonlinearities such as those observed in [4]. Analysis of the effect of harmonic distortion of a single UWB interferer at the receiver input is also presented.

UWB systems, with their wide front-ends, are susceptible to intermodulation (IM), harmonic distortion, and cross-modulation. A comprehensive analysis of the interaction of receiver nonlinearities and jammers present at the input of the receiver is needed to accurately predict the degradation in system parameters. For clarity and ease of design specification, these distortion components should be related to the well-known input-referred second-order intercept point (IIP_2) and input-referred third-order intercept point (IIP_3).

In this paper, we analyze the effect of receiver nonlinearities on a UWB multiband orthogonal frequency-division multiplexing (MB-OFDM) system. We consider the statistics of an

Manuscript received March 31, 2006; revised June 6, 2006. This work was supported by the University of California under a Discovery Grant.

M. Ranjan is with Qualcomm Inc., San Diego, CA 92121 USA (e-mail: mranjan@qualcomm.com; mahimranjan@yahoo.com).

L. E. Larson is with the Department of Electrical and Computer Engineering, University of California at San Diego, La Jolla, CA 92037 USA.

Color versions of Figs. 4, 7, 9, and 13 are available online at http://ieeexplore.ieee.org.

Digital Object Identifier 10.1109/TMTT.2006.882870

MB-OFDM system and derive closed-form expressions for the power spectral density (PSD) of different distortion components at the output resulting from receiver nonlinearities. The PSD obtained with these expressions is then compared with the results of a system simulation of a complete MB-OFDM system and its effect on the link budget of the system is analyzed.

The receiver and signal models are developed in Sections II and III. Sections V and VI analyze IM and harmonic distortion of wideband jammers. Analysis of cross-modulation of a narrowband jammer with a UWB interferer is presented in Section VII.

II. Receiver Model

We model the receiver front-end as a nonlinear system with its response to an input $x(t)$ given by

$$y(t) = c_1 x(t) + c_2 x^2(t) + c_3 x^3(t). \tag{1}$$

The transfer function will also consist of higher order terms, but in most situations, it is operated well below its 1-dB compression point, in which case, a third-order approximation models the receiver front-end quite accurately. AM–PM distortion is also negligible when a receiver is operated well below the 1-dB compression point and, thus, this effect can be neglected.

III. MB-OFDM Signal Model

MB-OFDM signals are quadrature phase-shift keying (QPSK) modulated and the symbols are carried over 128 carriers, occupying a total bandwidth of 528 MHz [1]. The transmitted RF MB-OFDM signal can be written as

$$r_{\rm rf}(t) = \mathrm{Re}\left(\sum_{k=0}^{N-1} r_k(t - kT_s)\exp(j2\pi f_{k\bmod 6} t)\right) \tag{2}$$

where $r_k(t)$ is the complex baseband variable representing the kth OFDM symbol and N is the total number of transmitted OFDM symbols. T_s is the symbol period. $f_{k\bmod 6}$ is the center frequency and $k\bmod 6$ represents the frequency hop algorithm that dynamically changes the center frequency of the MB-OFDM signal.

$r_k(t)$ is defined as

$$r_k(t) = \sum_{n=\frac{-N_s}{2}}^{\frac{N_s}{2}} C_n \exp(j2\pi n\Delta_f t) \tag{3}$$

where N_s is the total number of OFDM subcarriers, C_n is the complex baseband data, and Δ_f is the subcarrier spacing.

For a single frame (consisting of N_s subcarriers/symbols), the OFDM signal can be reduced to

$$\begin{aligned} r_{\rm rf}(t) &= A_{tx}\mathrm{rect}\left[\frac{t+\psi_t}{T_s}\right] \\ &\quad\times \sum_{n=\frac{-N_s}{2}}^{\frac{N_s}{2}} \{a_n \cos(((\omega_{tx}+n\Delta\omega)t+\theta) \\ &\qquad + b_n \sin((\omega_{tx}+n\Delta\omega)t+\theta))\} \end{aligned} \tag{4}$$

TABLE I
Assumed Receiver Specifications

Parameter	Value
Power Gain	20 dB
Noise Figure	4.9 dB

where A_{tx} is the rms amplitude of the transmitted signal, ω_{tx} is the angular frequency of the transmitted carrier, $\Delta\omega$ is the subcarrier spacing, a_n and b_n are the real and imaginary parts of the complex baseband signal C_n and take on the value $+/-1$ (QPSK modulation), θ is a random phase, ψ_t is a random time delay for the symbol, and $\mathrm{rect}[t/T_s]$ is defined as

$$\begin{aligned} \mathrm{rect}\left[\frac{t}{T_s}\right] &= 1, \qquad \text{if } \frac{-T_s}{2} < t < \frac{T_s}{2} \\ &= 0, \qquad \text{otherwise.} \end{aligned} \tag{5}$$

IV. MB-OFDM Received Power

For an MB-OFDM signal given by (4), its average power, for a normalizing impedance of 1 Ω, is give by [3]

$$P_{\rm in} = \frac{N_s A_{\rm TX}^2}{\pi}. \tag{6}$$

From [1], the maximum transmit power of an MB-OFDM transmitter is -10.3 dBm. For a receiver located 0.1 m away from the transmitter, the received power at the antenna would be approximately -35 dBm due to free-space path loss. Therefore, -35 dBm will be considered a representative maximum MB-OFDM signal level at the receiver antenna for all calculations.

For calculations in the remainder of this paper, the receiver front-end specifications assumed are summarized in Table I.

V. IM Distortion

Here, we consider the effects of IM distortion in MB-OFDM systems. IM distortion can arise from both second- and third-order nonlinearities, and we will consider the two separately.

A. Second-Order IM Distortion

Consider the following situation: the receiver is tuned to an MB-OFDM channel at 7128 MHz (Band 8). There are two other nearby transmitters transmitting at 3432 MHz (Band 1) and 3960 MHz (Band 2). Second-order nonlinearity in the receiver will result in these two unwanted received signals intermodulating and creating spurs at their sum and difference frequencies with the bandwidth of the spur spread to twice that of a single MB-OFDM signal. The sum frequency would be 7392 MHz, which will reduce the SNR for a receiver tuned to either Band 8 or Band 9 of an MB-OFDM system. This in-band spur will reduce the SNR and ultimately degrade system performance. Such a situation is depicted in Fig. 3.

Unlike narrowband systems, where second-order distortion at the front-end is important mainly due to the occurrence of a dc offset, second-order distortion in wideband systems such as MB-OFDM can directly result in degradation of system performance. An accurate prediction of this distortion product is required to correctly specify second-order distortion performance of the RF front-end.

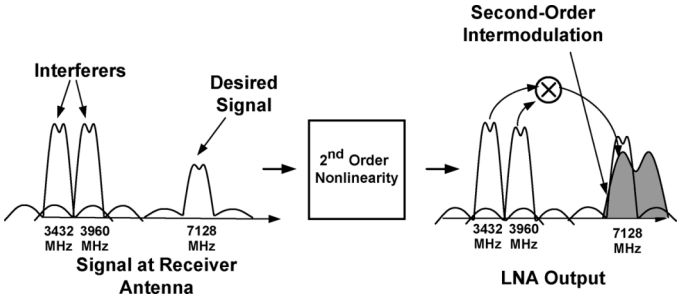

Fig. 3. Second-order IM scenario.

To derive an expression for this second-order IM PSD, we begin with the power series approximation for the low-noise amplifier (LNA) given by (1). The signal at the input of the receiver is a sum of two interfering MB-OFDM signals and can be written as

$$\begin{aligned} r_{\rm rf}(t) &= A_{\rm tx1}{\rm rect}\left[\frac{t+\psi_{t1}}{T_s}\right] \\ &\quad\times \sum_{n=\frac{-N_s}{2}}^{\frac{N_s}{2}} \{a_n \cos\left((\omega_{\rm tx1}+n\Delta\omega)t\right) \\ &\qquad +b_n \sin\left((\omega_{\rm tx1}+n\Delta\omega)t\right)\} \\ &\quad + A_{\rm tx2}{\rm rect}\left[\frac{t+\psi_{t2}}{T_s}\right] \\ &\quad\times \sum_{n=\frac{-N_s}{2}}^{\frac{N_s}{2}} \{c_n \cos\left((\omega_{\rm tx2}+n\Delta\omega)t+\theta\right) \\ &\qquad +d_n \sin\left((\omega_{\rm tx2}+n\Delta\omega)t+\theta\right)\} \end{aligned} \tag{7}$$

where $A_{\rm tx1}$ and $A_{\rm tx2}$ are the rms amplitudes of the two MB-OFDM signals and $\omega_{\rm tx1}$ and $\omega_{\rm tx2}$ are their angular frequencies. Substituting (7) into (1) and collecting terms around $\omega_{\rm tx1}+\omega_{\rm tx2}$, the second-order IM product is given by (8), shown at the bottom of this page. Since a_n, b_n, c_m, and d_m are random variables, to compute the PSD of this IM product, we need to compute the Fourier transform of the autocorrelation function of $S_{\rm IM2}(t)$ [5], which is given by

$$R_{ss}(\tau) = E\left\{S_{\rm IM2}(t)S_{\rm IM2}(t+\tau)\right\}. \tag{9}$$

Without loss of generality, we set the variable t to zero, corresponding to the assumption of a, b, c, and d being stationary random processes. We also state that a, b, c, and d are independent processes, we, therefore, have the following properties:

$$E\{a_k b_l c_n d_m\} = E\{a_k\}E\{b_l\}E\{c_n\}E\{d_m\} \tag{10}$$

$$\begin{aligned} E\{a_k a_n\} &= E\{b_k b_n\} = E\{c_k c_n\} = E\{d_k d_n\} \\ &= \delta_{kn} \qquad = 1, \qquad \text{if } k=n \\ &\qquad\qquad = 0, \qquad \text{otherwise.} \end{aligned} \tag{11}$$

Following analysis similar to [3], the PSD of the IM product can be written as (12), shown at bottom of this page.

To relate this PSD to the more familiar input IP2 ($\rm IIP_2$), c_2 in (1) can be replaced with

$$c_2 = \frac{c_1}{\rm IIP_2}. \tag{13}$$

To verify the validity of (12), a full system simulation of an MB-OFDM system was performed in MATLAB. The IM spectrum obtained was then compared with (12). The simulation was run for an MB-OFDM receiver, as described in [1], with an $\rm IIP_2$ of -10 dBm and undesired transmitter power of -20 dBm for each of the unwanted MB-OFDM transmitters. Simulated and calculated spectra are plotted in Fig. 4 and match very closely, verifying the validity of the prediction.

Using the IM power calculated above, the effect of receiver $\rm IIP_2$ on the total link budget can be calculated by adding this second-order IM power to the total in-band output noise power of the LNA. For the situation depicted in Fig. 3, this can be computed by integrating (12) from 6864 to 7392 MHz.

$$\begin{aligned} &S_{\rm IM2}(t) \\ &\quad = c_2 A_{\rm tx1} A_{\rm tx2}{\rm rect}\left[\frac{t+\psi_{t1}}{T_s}\right]{\rm rect}\left[\frac{t+\psi_{t2}}{T_s}\right] \\ &\qquad\times \sum_{m=\frac{-N_s}{2}}^{\frac{N_s}{2}} \sum_{n=\frac{-N_s}{2}}^{\frac{N_s}{2}} \{a_m c_n \cos\left((\omega_{\rm tx1}+\omega_{\rm tx2}+\Delta\omega(m+n)t+\theta\right)+a_m d_n \sin\left((\omega_{\rm tx1}+\omega_{\rm tx2}+\Delta\omega(m+n)t+\theta\right) \\ &\qquad\qquad +b_m c_n \sin\left((\omega_{\rm tx1}+\omega_{\rm tx2}+\Delta\omega(m+n)t+\theta\right)-b_m d_n \cos\left((\omega_{\rm tx1}+\omega_{\rm tx2}+\Delta\omega(m+n)t+\theta\right)\} \end{aligned} \tag{8}$$

$$\begin{aligned} {\rm PSD}_{\rm IM2}(\omega) = c_2^2 A_{\rm tx1}^2 A_{\rm tx2}^2 T_s \sum_{m=-\frac{N_s}{2}}^{\frac{N_s}{2}} \sum_{n=-\frac{N_s}{2}}^{\frac{N_s}{2}} &\left\{{\rm sinc}^2\left(\left(\omega+\left(\omega_{\rm tx1}+\omega_{\rm tx2}+\Delta\omega(m+n)\right)T_s\right)\right.\right. \\ &\left.\left.+{\rm sinc}^2\left(\left(\omega-\left(\omega_{\rm tx1}+\omega_{\rm tx2}+\Delta\omega(m+n)\right)T_s\right)\right\}\right. \end{aligned} \tag{12}$$

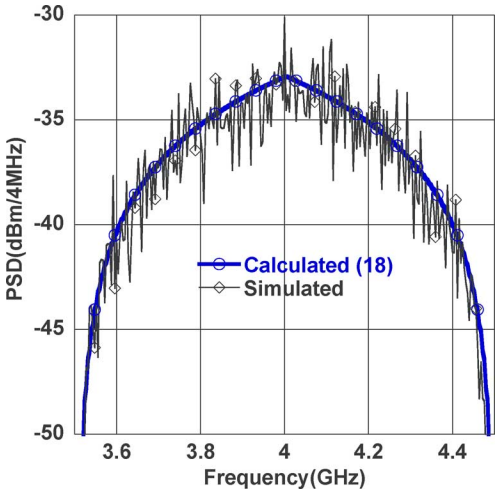

Fig. 4. Simulated and calculated second-order IM products. $\mathrm{IIP}_2 = -10$ dBm, UWB jammer powers $= -20$ dBm at 3.5 and 8 GHz.

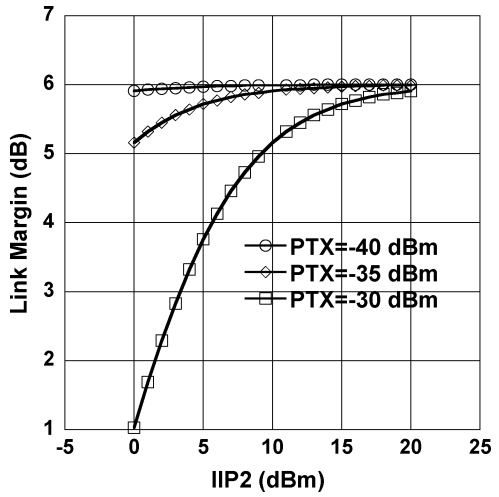

Fig. 5. Effect of second-order IM distortion on link margin (both jammers of equal magnitude).

Following the link budget analysis in [1] for a 110-Mb/s MB-OFDM system, the effect of second-order IM on total receiver link budget for the situation depicted in Fig. 3 is shown in Fig. 5. Fig. 5 shows the total receiver link margin as a function of IIP_2 in the presence of unwanted UWB transmitters transmitting at -30, -35, and -40 dBm. It can be seen that, in the absence of IM distortion, the total link budget is 6 dB, but this number degrades rapidly in the presence of strong unwanted MB-OFDM transmitters. Specifying the LNA IIP_2 without due consideration to IM can lead to inadequate system performance.

B. Third-Order IM Distortion

Here, we analyze the effect of third-order IM distortion on system performance. Third-order nonlinearities in the receiver can also result in unwanted signals falling in-band and reducing SNR. For example, transmitters at 3432 MHz (Band 1) and 3960 MHz (Band 2) can, in the presence of third-order nonlinearities, produce an IM product at 4488 MHz, which is in-band

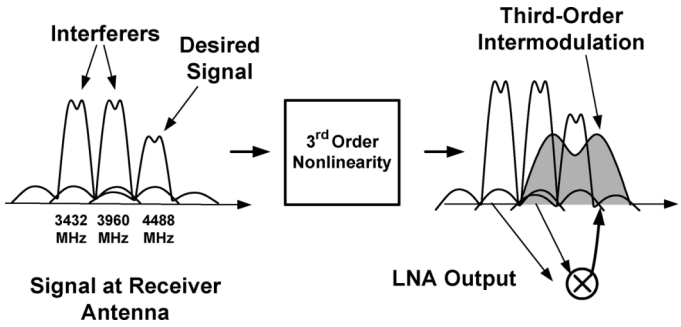

Fig. 6. Third-order IM scenario.

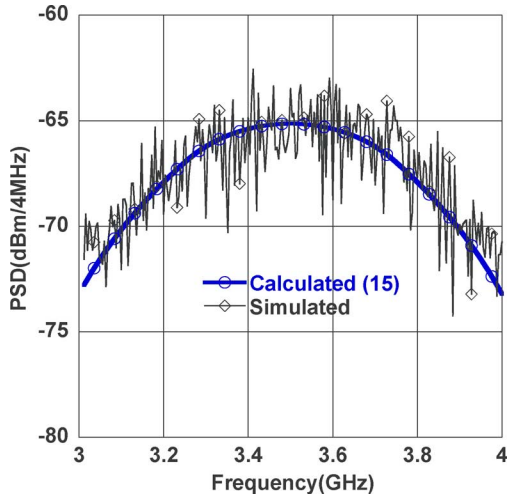

Fig. 7. Simulated and calculated third-order IM products. $\mathrm{IIP}_3 = -10$ dBm, UWB jammer powers $= -30$ dBm.

for a Group 1 MB-OFDM system. This situation is depicted in Fig. 6.

Representing the input signal by (7) and substituting into (1), the IM product at $2\omega_{\mathrm{tx1}} - \omega_{\mathrm{tx2}}$ is given by (14), shown at bottom of the following page.

Following analysis similar to [3], the PSD of this third-order IM product, computed as the autocorrelation function of (14), is given by (15), shown at the bottom of the following page.

To represent this cross-modulation component in terms of the more familiar IIP_3, we can represent c_3 as [6]

$$c_3^2 = \frac{4G}{9\mathrm{IIP}_3^2} \tag{16}$$

where G is the power gain of the LNA.

To evaluate the accuracy of (15), a full system simulation of an MB-OFDM receiver with an IIP_3 of -10 dBm was run with equal unwanted TX powers of -30 dBm. A comparison of simulated and calculated PSD of this third-order IM product is presented in Fig. 7 and the results match closely.

Using the IM power calculated in (15), the effect of receiver IIP_3, due to third-order IM of two nearby unwanted UWB transmitter jammers, on the total link budget can be calculated by adding this third-order IM power to the total output noise

power of the LNA. For the situation depicted in Fig. 6, this IM noise power can be computed by integrating (15) from 4224 to 4752 MHz.

Following the link budget analysis in [1] for a 110-Mb/s MB-OFDM system, the effect of third-order IM on the total receiver link budget for the situation depicted in Fig. 6 is shown in Fig. 8. Fig. 8 shows the receiver link margin for a receiver tuned to Band 3 of Group 1 as a function of IIP_3 in the presence of two unwanted UWB transmitters transmitting at -30, -35, and -40 dBm in Bands 1 and 2 of Group 1 of an MB-OFDM system.

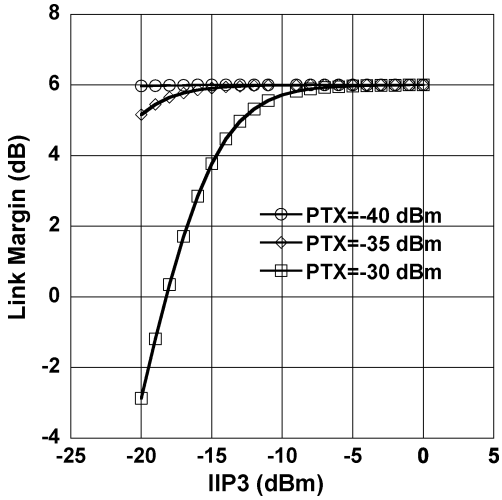

Fig. 8. Effect of third-order IM distortion on link margin.

VI. Harmonic Distortion

Unlike narrowband systems, harmonic distortion can also be a significant contributor to a degradation in the output SNR of the system. While with narrowband systems, harmonics of in-band signals are far away from the band of interest; in wide band systems such as MB-OFDM, the harmonics of the signal can also land in-band. For example, if the receiver is tuned to an MB-OFDM transmitter at 6.8 GHz, and there is a nearby transmitter present, transmitting at 3.4 GHz, second-order distortion in the receiver front-end will result in the second harmonic of the unwanted MB-OFDM transmitter falling in-band at 6.8 GHz. This will reduce the SNR at the output of the receiver front-end, and this effect needs to be quantized to accurately predict system performance in such situations.

Representing the input signal by (4) and substituting in (1), the second harmonic is given by (17), shown at the bottom of the following page.

Following analysis similar to [3], the PSD of this second harmonic, computed as the autocorrelation function of (17), is given by (18), shown at the bottom of the following page.

$$
\begin{aligned}
S_{\mathrm{IM3}}(t) = \frac{c_3}{4} A_{\mathrm{tx1}}^2 A_{\mathrm{tx2}} \mathrm{rect}\left[\frac{t+\psi_{t1}}{T_s}\right] \mathrm{rect}\left[\frac{t+\psi_{t2}}{T_s}\right] \\
\times \sum_{k=\frac{-N_s}{2}}^{\frac{N_s}{2}} \sum_{m=\frac{-N_s}{2}}^{\frac{N_s}{2}} \sum_{n=\frac{-N_s}{2}}^{\frac{N_s}{2}} \{3a_k b_m b_n [\cos\left(2\omega_{\mathrm{tx1}} - \omega_{\mathrm{tx2}} + \Delta\omega(m-n+k)\right)t + \theta) \\
+ \cos\left((2\omega_{\mathrm{tx1}} - \omega_{\mathrm{tx2}} + \Delta\omega(m-n-k)\right)t + \theta) \\
- \cos\left((2\omega_{\mathrm{tx1}} - \omega_{\mathrm{tx2}} + \Delta\omega(m+n-k)\right)t + \theta)] \\
+ 3a_m a_n b_k [-\sin\left((2\omega_{\mathrm{tx1}} - \omega_{\mathrm{tx2}} + \Delta\omega(m+n-k)\right)t + \theta) \\
+ \sin\left((2\omega_{\mathrm{tx1}} - \omega_{\mathrm{tx2}} + \Delta\omega(m-n+k)\right)t + \theta) \\
+ \sin\left((2\omega_{\mathrm{tx1}} - \omega_{\mathrm{tx2}} + \Delta\omega(-m+n+k)\right)t + \theta)] \\
+ a_k a_m a_n [\cos\left((2\omega_{\mathrm{tx1}} - \omega_{\mathrm{tx2}} + \Delta\omega\ (m+n-k)\right)t + \theta)) \\
+ \cos\left((2\omega_{\mathrm{tx1}} - \omega_{\mathrm{tx2}} + \Delta\omega(m-n+k)\right)t + \theta) \\
+ \cos\left((2\omega_{\mathrm{tx1}} - \omega_{\mathrm{tx2}} + \Delta\omega(-m+n+k)\right)t + \theta)] \\
+ b_k b_m b_n [\sin\left((2\omega_{\mathrm{tx1}} - \omega_{\mathrm{tx2}} + \Delta\omega(m+n-k)\right)t + \theta) \\
+ \sin\left((2\omega_{\mathrm{tx1}} - \omega_{\mathrm{tx2}} + \Delta\omega(m-n+k)\right)t + \theta) \\
+ \sin\left((2\omega_{\mathrm{tx1}} - \omega_{\mathrm{tx2}} + \Delta\omega(-m+n+k)\right)t + \theta)]\} \qquad (14)
\end{aligned}
$$

$$
\begin{aligned}
\mathrm{PSD}_{\mathrm{IM3}}(\omega) = \frac{9}{4} c_3^2 A_{\mathrm{tx1}}^4 A_{\mathrm{tx2}}^2 T_s \sum_{k=-\frac{N_s}{2}}^{\frac{N_s}{2}} \sum_{m=-\frac{N_s}{2}}^{\frac{N_s}{2}} \sum_{n=-\frac{N_s}{2}}^{\frac{N_s}{2}} \{\mathrm{sinc}^2\left(\left(\omega + \left(2\omega_{\mathrm{tx1}} - \omega_{\mathrm{tx2}} + \Delta\omega(m+n+k)\right)T_s\right)\right. \\
\left. + \mathrm{sinc}^2\left(\left(\omega - \left(2\omega_{\mathrm{tx1}} - \omega_{\mathrm{tx2}} + \Delta\omega(m+n+k)\right)T_s\right)\right\} \qquad (15)
\end{aligned}
$$

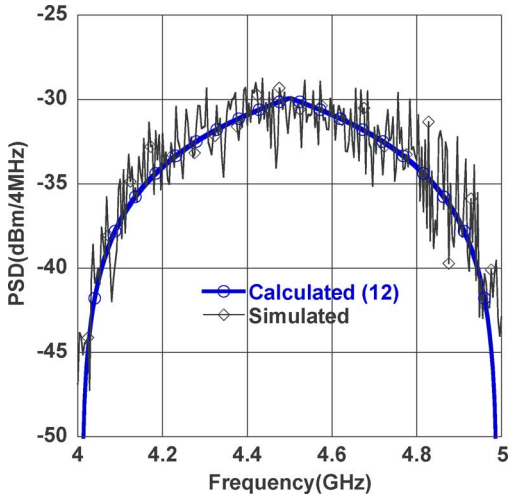

Fig. 9. Simulated and calculated second-order harmonic. $\mathrm{IIP}_2 = -10$ dBm, UWB jammer $= -10$ dBm at 4 GHz.

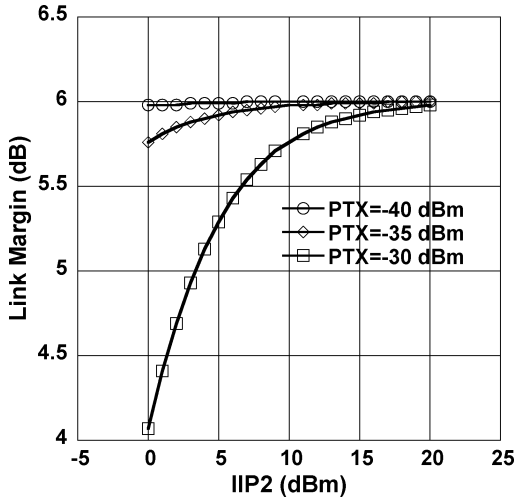

Fig. 10. Effect of second harmonic distortion on link margin.

Fig. 9 compares the simulated and calculated PSD of the second harmonic product for a UWB receiver with IIP_2 of -10 dBm and an unwanted UWB jammer at -10 dBm.

Again, to compute the degradation in link margin of a UWB receiver tuned to 6.8 GHz, due to the second harmonic of an unwanted UWB jammer at 3.4 GHz, we add the in-band noise power, computed by integrating (18) from 6.55 to 7.05 GHz to the output noise of the LNA. Fig. 10 shows the degradation in link margin due to second harmonic distortion in an MB-OFDM system.

VII. Cross-Modulation Distortion

A. UWB Interference Scenario

Consider the following interference situation, which can limit the performance of an MB-OFDM system: the receiver is tuned to an MB-OFDM transmitter transmitting in Band 1 of Group 1 (3.432-GHz center frequency)—this is the desired signal. There are two other undesired transmitters in the vicinity, which are: 1) a narrowband jammer (e.g., a relatively narrowband 3.0-GHz WiMAX) and 2) another MB-OFDM transmitter transmitting in one of the other bands in Group 1 (at 3.96 or 4.488 GHz). This situation is depicted in Fig. 11.

The receiver then accepts, in addition to the desired signal it is tuned to, another interfering input given by

$$s(t) = A_j \cos(\omega_j t) + A_{tx}\mathrm{rect}\left[\frac{t+\psi_t}{T_s}\right] \times \sum_{\frac{-N_s}{2}}^{\frac{N_s}{2}} \{a_n \cos((\omega_{tx} + \Delta\omega n)t + \theta) + b_n \sin((\omega_{tx} + \Delta\omega n)t) + \theta)\} \quad (19)$$

$$S_{\mathrm{HD2}}(t) = \frac{c_2}{2}A_{tx}^2\mathrm{rect}\left[\frac{t+\psi_t}{T_s}\right] \times \sum_{m=\frac{-N_s}{2}}^{\frac{N_s}{2}} \sum_{n=\frac{-N_s}{2}}^{\frac{N_s}{2}} \{a_m a_n \cos((2\omega_{tx} + \Delta\omega(m+n))t + \theta + b_m b_n \cos((2\omega_{tx} + \Delta\omega(m+n))t + \theta)) + 2a_m b_n \cos((2\omega_{tx} + \Delta\omega(m+n))t + \theta)\} \quad (17)$$

$$\mathrm{PSD}_{\mathrm{HD2}}(\omega) = \frac{c_2^2}{4}A_{tx}^4 T_s \sum_{m=-\frac{N_s}{2}}^{\frac{N_s}{2}} \left\{\mathrm{sinc}^2((\omega + (2\omega_{tx} + \Delta\omega(2m))T_s) + \mathrm{sinc}^2((\omega - (2\omega_{tx} + \Delta\omega(2m))T_s)\right\} + \frac{c_2^2}{2}A_{tx}^4 T_s \times \sum_{m=-\frac{N_s}{2}}^{\frac{N_s}{2}} \sum_{n=-\frac{N_s}{2}}^{\frac{N_s}{2}} \left\{\mathrm{sinc}^2((\omega + (2\omega_{tx} + \Delta\omega(m+n))T_s) + \mathrm{sinc}^2((\omega - (2\omega_{tx} + \Delta\omega(m+n))T_s)\right\} \quad (18)$$

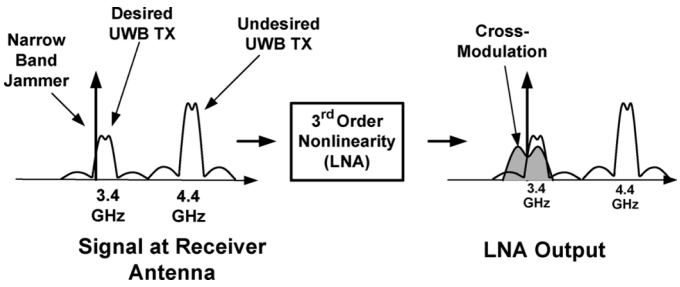

Fig. 11. Typical UWB cross-modulation scenario.

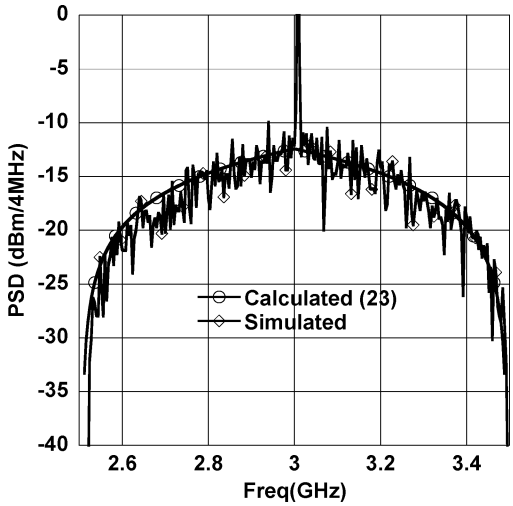

Fig. 12. Simulated and calculated cross-modulation products (from [3]). $\mathrm{IIP}_3 = -10$ dBm, Narrowband jammer power $= -10$ dBm, UWB jammer power $= -10$ dBm.

where ω_j is the frequency of the narrowband jammer and ω_{tx} is the center frequency of the second unwanted MB-OFDM transmitter. A_j is the amplitude of the narrowband jammer, A_{tx} is the rms amplitude of the second unwanted MB-OFDM transmitter, and θ is a random phase. The first term in (19) represents the narrowband jammer and the second term represents the unwanted MB-OFDM transmitter.

B. Cross-Modulation

Substituting (19) into (1), it can be shown that the cross-modulation product (at frequencies around ω_j) is given by [3]

$$\begin{aligned} x\mathrm{mod}(t) = \frac{c_3}{4} A_j A_{tx}^2 \mathrm{rect}\left[\frac{t+\psi_t}{T_s}\right] \\ \times \sum_{m=\frac{-N_s}{2}}^{\frac{N_s}{2}} \sum_{n=\frac{-N_s}{2}}^{\frac{N_s}{2}} (a_m a_n + b_m b_n) \\ \times \{\cos\left((\omega_j + \Delta\omega(m-n))\, t + \theta\right) \\ + \cos\left((\omega_j - \Delta\omega(m-n))\, t + \theta\right)\}. \end{aligned} \quad (20)$$

Since a_n and b_m are random variables, to compute the PSD of the cross-modulation, we need to compute the Fourier transform of the autocorrelation function of $x\mathrm{mod}(t)$.

Using the properties in (10) and (11), the autocorrelation function can be simplified to

$$\begin{aligned} R_{xx}(\tau) = \frac{c_3^2}{2} \left(A_j A_{tx}^2\right)^2 \Delta_{T_s}(\tau) \\ \times \sum_{m=\frac{-N_s}{2}}^{\frac{N_s}{2}} \sum_{n=\frac{-N_s}{2}}^{\frac{N_s}{2}} \{\cos\left((\omega_j + \Delta\omega(m-n))\, \tau\right)\} \end{aligned} \quad (21)$$

where $\Delta_{T_s}(\tau)$ is defined as

$$\begin{aligned} \Delta_{T_s}(\tau) &= 1 - \frac{|\tau|}{T_s}, \qquad \text{if } -T_s < \tau < T_s \\ &= 0, \qquad \text{otherwise.} \end{aligned} \quad (22)$$

The PSD of the cross-modulation component can be obtained by taking the Fourier transform of (21). Taking the Fourier transform of (21), the PSD is given by (23), shown at the bottom of this page. It is clear from (23) the spectrum of the jammer is spread to twice the bandwidth of the wideband signal. If the jammer is close enough to the desired band, this cross-modulation spectrum can land on top of the desired signal, reducing the SNR, with the extent of the reduction in SNR depending on the IIP_3 and the narrowband and wideband jammer powers.

To verify the validity of (23), a full system simulation of an MB-OFDM system was performed in MATLAB. The cross-modulation spectrum obtained was then compared with the prediction of (23). The simulation was run for an MB-OFDM receiver, as described in [1], with an IIP_3 of -10 dBm, input narrowband jammer power of -10 dBm, and undesired wideband jammer power of -10 dBm. Simulated and calculated spectra are plotted in Fig. 12 and match very closely, verifying the validity of the prediction.

C. Effect of Single-Tone Approximation

Since in a real-world application the narrowband jammer in (19) would be modulated, it is of interest to compare the cross-modulation spectrum when the jammer is a single tone and when it is modulated. Simulations were performed to compare the calculated cross-modulation spectrum with a single-tone narrowband jammer, an FM modulated jammer with 5-MHz bandwidth, and an FM modulated jammer with 10-MHz bandwidth. The results of these simulations are plotted in Fig. 13. It can be seen that the modulated jammers spread the cross-modulation

$$\mathrm{PSD}_{\mathrm{XMOD}}(\omega) = \frac{c_3^2}{2} \left(A_j A_{tx}^2\right)^2 T_s \sum_{m=-\frac{N_s}{2}}^{\frac{N_s}{2}} \sum_{n=-\frac{N_s}{2}}^{\frac{N_s}{2}} \mathrm{sinc}^2\left((\omega + (\omega_j + \Delta\omega(m-n))\, T_s\right) + \mathrm{sinc}^2\left((\omega - (\omega_j + \Delta\omega(m-n))\, T_s\right) \quad (23)$$

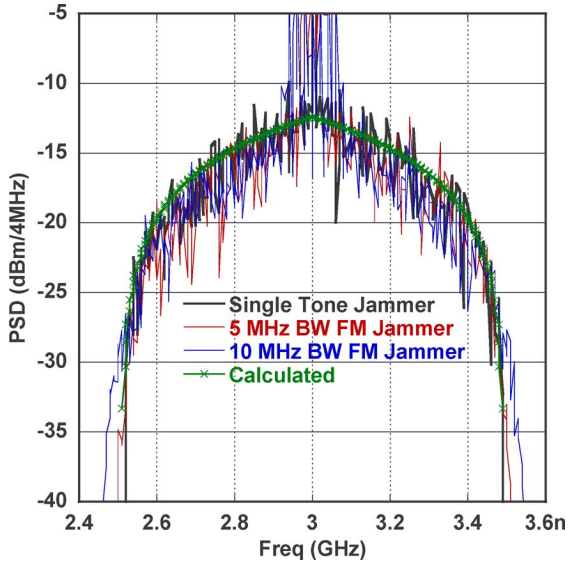

Fig. 13. Simulated and calculated cross-modulation products (from [3]). $\mathrm{IIP}_3 = -10$ dBm, Narrowband jammer power $= -10$ dBm, UWB jammer power $= -10$ dBm.

spectrum by approximately their modulation bandwidth. Therefore, for relatively narrowband jammers, the cross-modulation spectrum obtained correlates very well with the spectrum calculated using a single tone approximation of (19).

D. Effect of Cross-Modulation on Link Margin

To evaluate the effect of this spread jammer on the total SNR at the output of the LNA, we need to integrate (23) within the bandwidth of the desired received signal.

For example, consider the case when the receiver is tuned to an MB-OFDM transmitter transmitting in Band 1 of Group 1 (3.15–3.65 GHz). There is also present another MB-OFDM transmitter in the vicinity transmitting in Band 3 of Group 1 (4.15–4.65 GHz) and a narrowband transmitter transmitting at 3.0 GHz. Since the cross-modulation product is twice the bandwidth of the MB-OFDM signal, it will occupy 2.5–3.5 GHz. This means that the cross-modulation product overlaps with the desired channel and we need to integrate (23) from 3.15 to 3.5 GHz to calculate the total noise power contributed by this cross-modulation product.

To compare the total noise power, (23) was numerically integrated with $\mathrm{IIP}_3 = -10$ dBm, $P_j = -10$ dBm, and $P_{\mathrm{TX}} = -10$ dBm. MATLAB simulations show the complete noise power to be 2.35 dBm and numerical integration of (23) revealed excellent agreement with a total noise power of 2.31 dBm.

Using the cross-modulation power calculated above, the effect of receiver IIP_3 on the total link budget can be calculated by adding this cross-modulation power to the total output noise power of the LNA. Using the link budget analysis in [1] for a 110-Mb/s MB-OFDM system, the effect of cross-modulation on total receiver link budget is shown in Fig. 14–16. These figures show the total receiver link margin for the situation described above, as a function of IIP_3 in the presence of a narrowband jammer of -20, -30, and -40 dBm, when the wideband jammers are at -30, -35, and -40 dBm. It can be seen that, in the absence of cross-modulation distortion, the total link budget

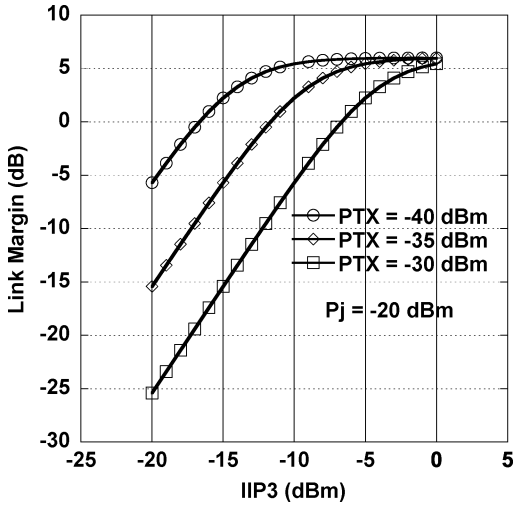

Fig. 14. Receiver link margin versus IIP_3 in the presence of cross-modulation single-tone jammer power $= -20$ dBm. Link margin in the absence of cross-modulation $= 6$ dB.

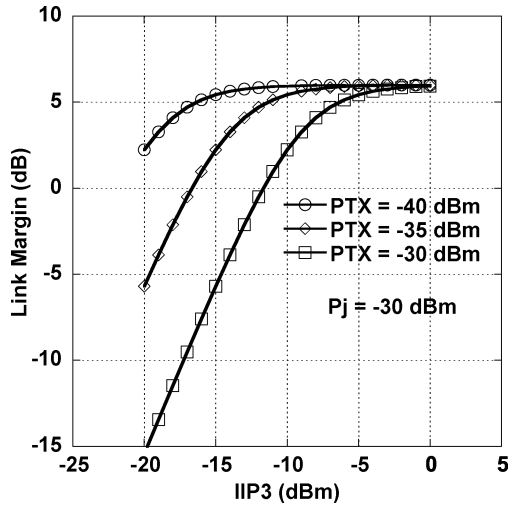

Fig. 15. Receiver link margin versus IIP_3 in the presence of cross-modulation (from [3]) single-tone jammer power $= -30$ dBm. Link margin in the absence of cross-modulation $= 6$ dB.

is 6 dB, but this number degrades rapidly in the presence of a strong narrowband jammer. Specifying the LNA IIP_3 without due consideration to cross-modulation can lead to inadequate system performance.

VIII. Example Calculation

The goal of this paper is to present a framework for system designers to easily specify the linearity requirements of an MB-OFDM-based UWB receiver. This can be achieved either with full system simulations or through analytical methods. The RF simulation of MB-OFDM systems is very computationally intensive due to the large fractional bandwidth of the system, and also due to the statistical nature of the signal, which makes it necessary to simulate multiple random symbols to obtain an average value for the distortion products. The expressions derived thus far ease the analysis to a simple numerical integration.

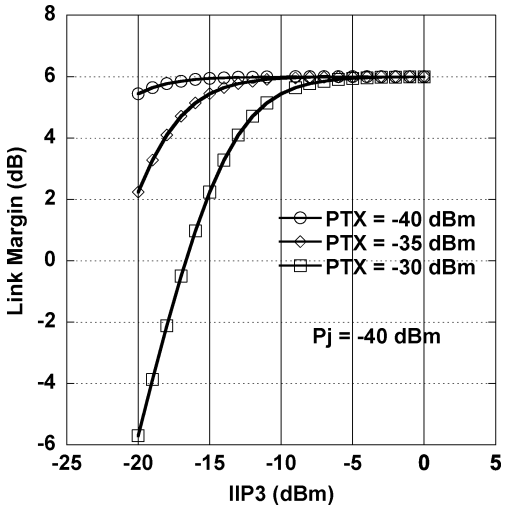

Fig. 16. Receiver link margin versus IIP_3 in the presence of cross-modulation single-tone jammer power $= -40$ dBm. Link margin in the absence of cross-modulation $= 6$ dB.

To further reduce computation time, estimates of the above distortion products can also be made. We demonstrate a method of arriving at this estimate by computing the noise power for the cross-modulation scenario of Fig. 11. We assume, without significant loss of accuracy, that the total noise power in each sinc function in the summation in (23) lies inside the bandwidth of integration. The integral of each term inside the summation also reduces to $1/2\pi T_s$.

Now, for the frequency of interest (3.4 GHz), we need to consider the cross-modulation products between 3.15–3.5 GHz. In the summation in (23), the term $\mathrm{sinc}^2((\omega + (\omega_j + \Delta\omega(m - n))T_s)$ occurs $N_s - (m-n)$ times, and there are two sinc terms in the summation.

Therefore, for the given frequencies and assuming $\Delta_f = 4$ MHz (MB-OFDM),

$$3.15G = f_j + 37\Delta_f \quad 3.5G = f_j + 124\Delta_f \tag{24}$$

the summation in (23) reduces to

$$n = (N_s - 37) + (N_s - 38) + \cdots + (N_s - 124). \tag{25}$$

For $N_s = 128$ (MB-OFDM) [see (3)], this results in $n = 3652$. We, therefore, need to substitute $2 \times 3652 \times (1/2\pi T_s)$ for the summation in (23) to compute the total noise power. Using the above-mentioned values for IIP_3, P_j, and P_{TX}, this gives a total noise power of 0.4 dBm, which is in good agreement with the previous result of 2.31 dBm, based on numerical integration.

This method of cross-modulation estimation reduces the complicated problem of wideband RF simulation to a simple summation, reducing the simulation time from hours to almost instantaneous. Even without the above approximation, the cross-modulation formula (23) reduces the problem drastically from a full system simulation and numerical integration of output power. For multiple scenarios (varying TX or jammer powers, receiver IIP_3 or IIP_2), one would need to run a simulation for each situation to determine its effect on receiver SNR. However, using (23), after the initial numerical integration of the terms inside the summation of the PSD equation, cross-modulation power can be immediately calculated for different scenarios.

IX. Inaccuracies Resulting from Use of Two-Tone IM Test in UWB Systems

A very simple and attractive way of estimating harmonic and IM components in narrowband systems is by predicting them through a traditional two-tone analysis. For example, the third-order IM product of a narrowband system can be approximated by using the well-known formula

$$\mathrm{IIP}_3 = P_{\mathrm{in}} + \frac{\Delta_p}{2} \tag{26}$$

where P_{in} is the power of the single tones at the input and Δ_p is the observed difference between the single tone output and the IM3 product. For example, for a receiver with an IIP_3 of -10 dBm, gain of 15 dB and input single-tone powers of -30 dBm, this would yield an output IM3 power of -55 dBm. However, spread-spectrum analysis and simulation of this receiver show the output IM power in a single MB-OFDM receive band to be -50 dBm. This example demonstrates the high levels of inaccuracy that can be introduced in UWB system analysis if single-tone approximations of these receivers are utilized to predict system performance. The more accurate analysis presented here presents a realistic estimate of the nonlinear distortion that can be expected in these systems.

X. Conclusion

In this paper, we have analyzed the effect of receiver nonlinearities on the performance of MB-OFDM-based UWB systems. Both narrowband and wideband jammers were considered. Analytical expressions relating cross-modulation, IM, and harmonic distortion power spectral densities with jammer powers and receiver nonlinearities were derived. The PSD of these distortion products was compared with that obtained from full system simulations, and simulations were observed to closely match with analytical results. It was shown, with the help of an example, that single-tone approximation of these systems can result in high levels of inaccuracies and true wideband analysis, presented in this paper, is necessary for accurate estimation of system parameters. The equations obtained were used to calculate degradation in the link budget of the system for different scenarios. An approximation method to speed calculation of these expressions was also presented.

Acknowledgment

The authors wish to acknowledge the assistance and support of Qualcomm Inc., San Diego, CA, the Center for Wireless Communication, University of California at San Diego, La Jolla, Dr. J. Foerster, Intel, Hillsboro, OR, and Prof. L. Milstein, University of California at San Diego, La Jolla, for valuable discussions.

References

[1] A. Batra, J. Balakrishnan, R. Aiello, J. Foerster, and A. Dabak, "Design of a multiband OFDM system for realistic UWB channel environments," *IEEE Trans. Microw. Theory Tech.*, vol. 52, no. 12, pp. 2123–2138, Sep. 2004.

[2] A. Ghosh, D. R. Walter, J. G. Andrews, and R. Chen, "Broadband wireless access with WiMax/802.16: Current performance benchmarks and future potential," *IEEE Commun. Mag.*, vol. 43, no. 2, pp. 129–136, Feb. 2005.
[3] M. Ranjan and L. Larson, "An analysis of cross-modulation distortion in ultra wideband OFDM receivers," in *IEEE MTT-S Int. Microw. Symp. Dig.*, Jun. 2006, [CD ROM].
[4] D. Leenaerts, "Circuit design for ultra-wideband," presented at the CICC RF Educ. Session, 2005.
[5] J. Proakis, *Digital Communications*, 4th ed. New York: McGraw-Hill, 2000.
[6] V. Aparin and L. Larson, "Analysis and reduction of cross-modulation distortion in CDMA receivers," *IEEE Trans. Microw. Theory Tech.*, vol. 51, no. 12, pp. 1591–1602, May 2003.
[7] ——, "Analysis of cross-modulation in W-CDMA receivers," in *IEEE MTT-S Int. Microw. Symp. Dig.*, Jun. 2004, vol. 2, pp. 787–790.

Mahim Ranjan (S'99–M'02) received the Bachelor's degree in electrical engineering from the Indian Institute of Technology, Bombay, India, in 1999, the Master's degree in electrical and computer engineering from the University of California at San Diego, La Jolla, in 2000, and is currently working toward the Ph.D. degree at the University of California.

From 2001 to 2004, he was an Engineer with Magis Networks, San Diego, CA, where he was involved with RF transceivers for wireless multimedia. He is currently a Senior Design Engineer with Qualcomm Inc., San Diego, CA, where he designs RF transceivers for cellular applications.

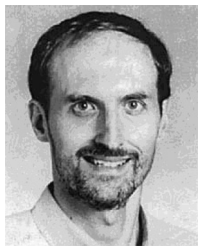

Lawrence E. Larson (S'82–M'86–SM'90–F'00) received the B.S. and M. Eng. degrees in electrical engineering from Cornell University, Ithaca, NY, in 1979 and 1980, respectively, and the Ph.D. degree in electrical engineering and MBA degree from the University of California at Los Angeles (UCLA), in 1986 and 1996, respectively.

From 1980 to 1996, he was with Hughes Research Laboratories, Malibu, CA, where he directed the development of high-frequency microelectronics in GaAs, InP, and Si/SiGe and microelectromechanical systems (MEMS) technologies. In 1996, he joined the faculty of the University of California at San Diego (UCSD), La Jolla, where he is the Inaugural Holder of the Communications Industry Chair. He is currently Director of the UCSD Center for Wireless Communications. During the 2000–2001 academic year, he was on leave with IBM Research, San Diego, CA, where he directed the development of RF integrated circuits (RFICs) for third-generation (3G) applications. During the 2004–2005 academic year, he was a Visiting Professor with the Technical University of Delft (TU Delft), Delft, Netherlands. He has authored or coauthored over 250 papers. He holds 31 U.S. patents.

Dr. Larson was the recipient of the 1995 Hughes Electronics Sector Patent Award for his work on RF MEMS technology. He was corecipient of the 1996 Lawrence A. Hyland Patent Award of Hughes Electronics for his work on low-noise millimeter-wave high electron-mobility transistors (HEMTs), the 1999 IBM Microelectronics Excellence Award for his work in Si/SiGe HBT technology, and the 2003 Custom Integrated Circuits Conference Best Invited Paper Award.